Vicarious Calibration of an Ocean Salinity Radiometer from Low Earth Orbit

CHRISTOPHER S. RUF

Department of Atmospheric, Oceanic and Space Sciences, University of Michigan, Ann Arbor, Michigan

(Manuscript received 5 April 2002, in final form 7 January 2003)

ABSTRACT

Statistical properties of the brightness temperature (T_B) measured by a low-earth-orbiting radiometer operating at 1.4 GHz are considered as a means of calibrating and validating the sensor. Mapping of ocean salinity by such an instrument requires that its calibration be extremely stable over time. Whether certain statistical properties of the measurements are stationary (time invariant) enough to be of value as benchmarks to which the calibration can be referenced is considered. The global minimum, maximum, and average T_B are considered, together with a vicarious cold T_B statistic that makes use of a sharp lower bound on naturally occurring values for T_B. Examination of simulated global distributions of the T_B measurements suggests several things about the stationarity (or lack thereof) of the statistics in question. Global minima can vary widely due to instrument noise and are not a reliable calibration reference. Global maxima are strongly influenced by a number of environmental factors as well as by instrument noise and are even less stationary than the minima. Global averages are largely insensitive to instrument noise and, in most cases, to environmental conditions as well. The global average T_B varies at only the 0.1-K rms level except in cases of anomalously high winds, when it can increase considerably more. The vicarious cold T_B is similarly insensitive to instrument effects and most environmental factors. It is not significantly affected by high wind conditions. The stability of the vicarious cold T_B is, however, found to be sensitive at the several tenths of a kelvin level to variations in the background cold space brightness. The global average is much less sensitive to this parameter, so using the two approaches together should be mutually beneficial.

1. Introduction

Global mapping of sea surface salinity (SSS) has been identified as a critical unmet need of the oceanography and climate studies communities (Lagerloef et al. 1995). SSS maps identify variations in water density and, hence, ocean circulation and heat transport patterns. SSS also helps to resolve the energy flux at the air–sea interface that is related to evaporation and precipitation. One candidate methodology for providing global maps of SSS with acceptable spatial and temporal resolution is microwave radiometry in low earth orbit (Swift and McIntosh 1983). Aircraft radiometer measurements at 1.41 GHz have clearly demonstrated the potential to remotely sense SSS with the high level of accuracy and precision that are needed to be of real value to the oceanography and climate studies communities (Le Vine et al. 1998). Detailed spacecraft design studies have quantified the requirements on radiometer stability that will be needed in order to provide similarly accurate and precise SSS retrievals from low earth orbit (Yueh et al. 2001). Here, radiometer stability can be defined by considering its measurements to be composed of an ideal, constant value to which is added both a slowly varying component and a component that is decorrelated between samples. The magnitude and timescale of the slowly varying component determine the stability of the radiometer. On orbit radiometer stability is needed at the 0.05–0.1-K level over periods of weeks to successfully measure SSS (Koblinsky 2002). This is roughly an order of magnitude more stringent than has been demonstrated on typical radiometer flight missions. Conventional methods of radiometer calibration cannot be relied on to provide the necessary level of performance. A new method of calibration has recently been developed for radiometers operating at higher microwave frequencies of 18–37 GHz (Ruf 2000). Calibration stability has been demonstrated at the several tenths of kelvins level over periods of years. The method is evaluated here to see how much the stability will improve if used at the lower frequency of 1.41 GHz and if the timescale of stability is reduced from years to weeks.

The manner in which the microwave brightness temperature (T_B) of the ocean varies as a function of sea surface temperature (SST), salinity, near-surface wind speed (u), and atmospheric opacity can be taken advantage of as a source of vicarious calibration for an orbiting microwave radiometer. For every microwave frequency, polarization, and incidence angle there is a

Corresponding author address: Dr. Christopher S. Ruf, Department of Atmospheric, Oceanic and Space Sciences, University of Michigan, Space Research Bldg., 2455 Hayward, Ann Arbor, MI 48109-2143.
E-mail: cruf@umich.edu

unique combination of SST and SSS at which the T_B of an ideal, flat ocean surface is a minimum. Departures of SST and SSS from that point, as well as all variations in u and atmospheric opacity, will tend to increase the T_B observed by a downward-looking radiometer in earth orbit above its theoretical minimum. An inverse cumulative distribution function (ICDF) for T_B can be constructed that has the property that

$$\text{ICDF}(x) = T_B \quad \text{for } 0 \le x \le 100\% \tag{1}$$

provided x% of the measurements have values below T_B. The ICDF is the inverse of the standard cumulative distribution function (CDF, the definite integral of the probability density function for T_B) in the sense that $T_B = \text{ICDF}[\text{CDF}(T_B)]$. The ICDF can be used to solve for the highest T_B for which $x = 0\%$. This statistic will henceforth be referred to as the vicarious cold T_B. (Details of the algorithms used to construct the ICDF from an ensemble of T_B measurements and to estimate the vicarious cold T_B from it are given in appendix A.) This vicarious cold T_B has been successfully used as a calibration referenced for the TOPEX Microwave Radiometer (TMR) with channels of 18, 21, and 37 GHz at a nadir angle of incidence (Ruf 2000). It has been found to be repeatable to better than 0.3-K rms over a 6-yr period.

Two characteristics of this method of vicarious calibration are important to recognize. First, the conditions for minimum T_B (a specific combination of SST and SSS together with zero winds and a transparent atmosphere) are never really present, nor do they need to be. It is sufficient that the lower bound on T_B exists in principle and that a significant number of measurements are made in the near vicinity of the minimum. In fact, actual measurements are occasionally recorded below the minimum due to the effects of additive noise and random calibration errors. Extrapolation of the ICDF from a very large set of measurements (in our case covering all of $x = 1\%$–10%) back to the point $x = 0\%$ tends to correct for these random effects, provided they are unbiased. (Thus, biased calibration effects can be very quickly identified by this method.) It is much less reliable to simply select a single ICDF value (e.g., ICDF at $x = 0.1\%$) as a vicarious T_B calibration reference.

A second important characteristic of this method is its ability to adapt to significant changes in the statistical distribution of T_Bs. In the case of TMR, independent ICDFs were derived every 10 days of flight data. Very noticeable changes were observed in the relationship between x and ICDF(x) over the range $x = 1\%$–10%. This was particularly true of the TMR 21-GHz channel during the 1997–98 ENSO event. The shift in statistics during that period was likely a result of variations in the joint probability of occurrence of SST and atmospheric water vapor. Due to the changes in shape of the ICDF, the extrapolation back to ICDF ($x = 0\%$) was performed dynamically by adjusting to the shape of the ICDF independently every 10 days (see Ruf 2000 for details). Thus, while the shape of the ICDF changed significantly during 1997–98, the highest T_B at which $x = 0\%$ did not.

Application of the vicarious cold T_B method to an L-band radiometer operating at 1.4135 GHz is considered here. The general behavior of T_B versus SST, SSS, polarization, and incidence angle are shown in Figs. 1 and 2. (Details of the forward model used to estimate T_B from the geophysical state are given in section 2 below.) In each of the figures, the T_B assumes an ideal, flat ocean surface, together with a water vapor free atmosphere (assuming O_2 absorption/emission only) and a downwelling cold space brightness of 6 K incident on the top of the atmosphere. The effects of atmospheric water vapor and surface wind roughening and foam are neglected here but are considered later. Figure 1 show the dependence of T_{Bh} (H polarized), T_{Bv} (V polarized), and $T_{B1} = (T_{Bh} + T_{Bv})/2$ (the first Stokes polarization) on SST for a typical SSS value of 34 ppt. The T_{B1} polarization is considered here because it is insensitive to Faraday rotation. In all three cases, the behavior of T_B differs markedly from that at the higher microwave frequencies considered in Ruf (2000). A ''natural'' minimum T_B existed at the higher frequencies for specific values of SST. Here at L band, there is no such natural minimum; in fact an apparent maximum T_B exists near SST = 15°–18°C. (There would, in practice, be no such maximum present due to the many other environmental factors that tend to increase T_B above the levels shown in Fig. 1.) At L band, the lowest T_Bs occur at the warmest and coldest values of SST, with the coldest SSTs producing slightly lower T_Bs. In addition, the additive effects on T_B of other environmental factors will also tend to be smallest at the coldest SSTs. Seawater in the open ocean has a fairly sharp lower bound at −2°C, below which ice forms and T_B increases. The dependence of T_B on SSS is shown in Fig. 2 at an SST value of −2°C. At all incidence angles and polarizations, T_B decreases monotonically with increasing SSS. Thus, the occurrence of coldest T_B will generally coincide with the coldest and saltiest ocean conditions.

The presence of a natural minimum T_B, in which the SST that produces a minimum T_B is in the range of naturally occurring values, does not occur at L band. It begins to occur as the frequency increases to X band. For example, a minimum T_B occurs when SST = 0°C at approximately 10 GHz for nadir incidence. At 53° incidence, the same situation occurs at approximately 10 GHz for H-pol and 12 GHz for V-pol. At higher frequencies, the SST that produces a minimum T_B is above 0°C. At lower frequencies, the corresponding SST is below 0°C and, in particular, is below −2°C at typical S- and C-band frequencies used in microwave radiometry. Note, also, that at X band the dependence of the minimum T_B on SSS is approximately 0.02 K psu^{-1} and it becomes even weaker at higher frequencies. Thus, application of the vicarious cold T_B method at X band

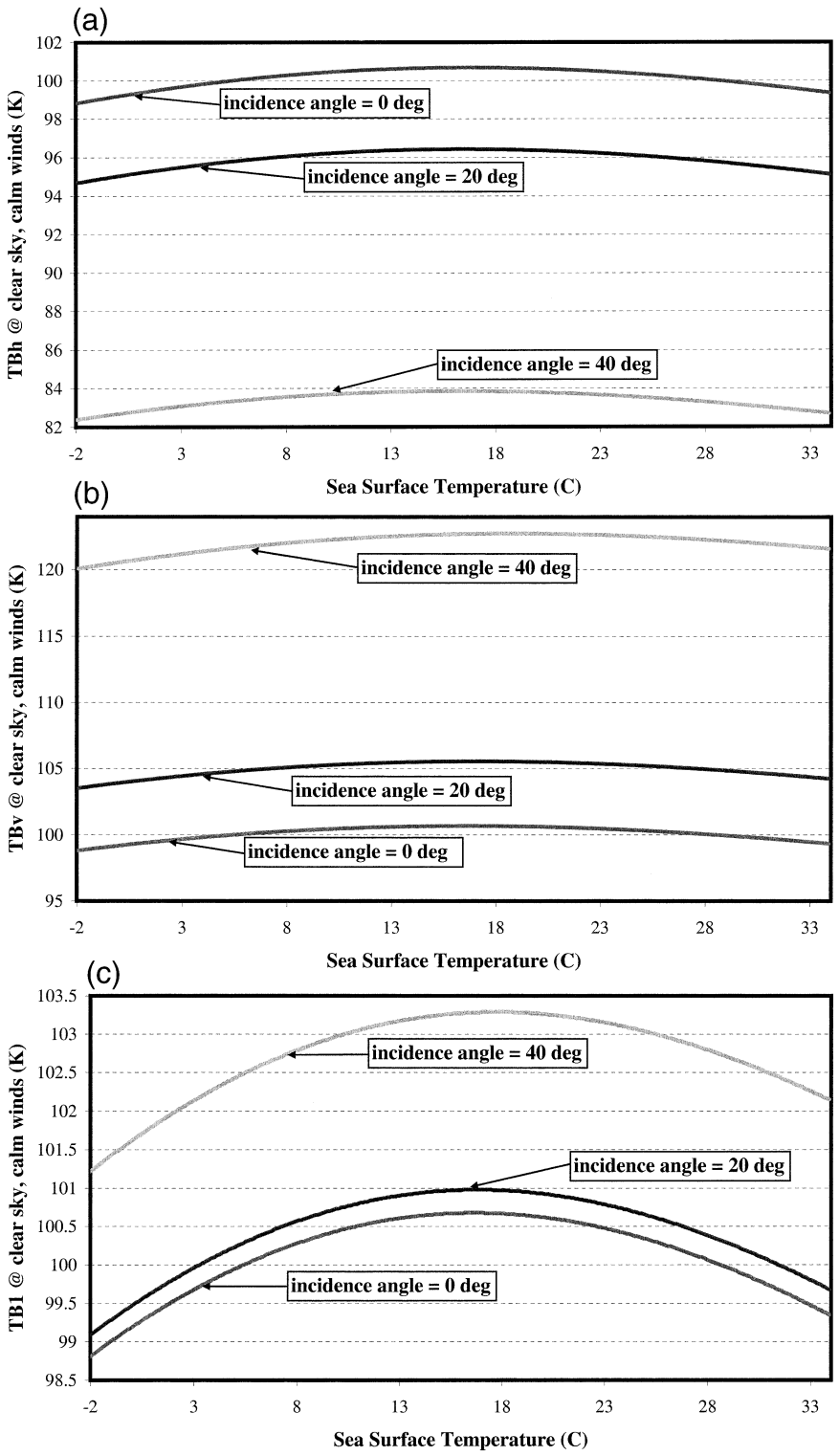

FIG. 1. The T_B over ocean at 1.4135-GHz (a) H-pol, (b) V-pol, and (c) first Stokes $(T_{Bv} + T_{Bh})/2$ pol vs SST and incidence angle, assuming an ideal, flat ocean surface and no water vapor.

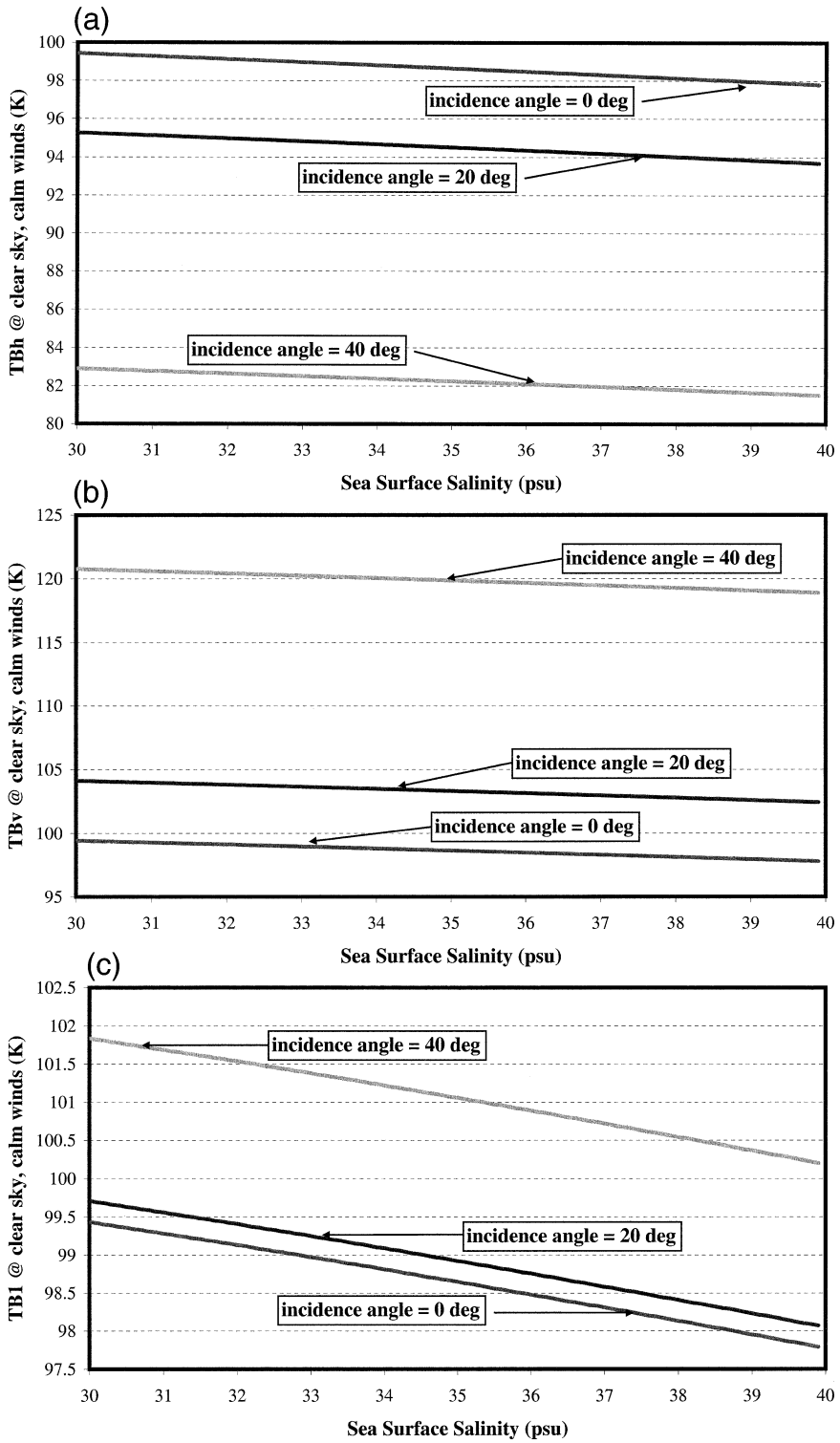

FIG. 2. The T_B over ocean at 1.4135-GHz (a) H-pol, (b) V-pol, and (c) first Stokes pol vs SSS and incidence angle, assuming an ideal, flat ocean surface and no water vapor.

and above would closely resemble the experience with TMR (Ruf 2000).

2. Forward model for brightness temperature

The forward model that estimates T_B from the geophysical state comprises several components. The dependence of the ocean's complex dielectric constant on SST, SSS, and microwave frequency follows the model developed by Stogryn (1997). This model has a relatively small difference in behavior from those by Klein and Swift (1977) and Ellison et al. (1998) at L band. The differences are more pronounced at higher microwave frequencies. The dependence of the ocean surface emissivity on surface wind speed (due to roughening and the presence of foam) is modeled by the following semiempirical relationship:

$$\varepsilon_h = \varepsilon_{h,0} + u(0.0007 + 0.000\,015\theta_{\text{inc}})$$
$$\varepsilon_v = \varepsilon_{v,0} + 0.0007u, \quad (2)$$

where ε_p is the emissivity at polarization $p = h$ or v; $\varepsilon_{p,0}$ is the emissivity at polarization p of an ideal, flat ocean surface using Stogryn (1997) for ocean dielectric constant; u is the neutral stability near-surface wind speed; and θ_{inc} is the incidence angle in units of degrees. This model for wind-induced excess emissivity follows from Blume et al. (1977) for nadir sensitivity, together with an estimated extrapolation to off-nadir incidence using a two-scale surface emission model (F. J. Wentz 2001, personal communication).

Atmospheric opacity at L band is modeled using the following relationship:

$$\tau = (0.009\,364 + 0.000\,024\,127V)\sec(\theta_{\text{inc}}), \quad (3)$$

where τ is the line-of-sight opacity through the atmosphere in units of nepers and V is the zenith-integrated water vapor burden present in the atmospheric column in units of centimeters. Equation (3) was derived by performing a linear least squares regression fit between L- band opacities and corresponding values of integrated water vapor burden derived from a large ensemble of globally distributed radiosonde profiles over the ocean. Atmospheric upwelling and downwelling brightness are, respectively, modeled using

$$T_{B,\text{UP}} = (1 - e^{-\tau})(\text{SST} + 258.15) \quad \text{and}$$
$$T_{B,\text{DOWN}} = (1 - e^{-\tau})(\text{SST} + 263.15), \quad (4)$$

where SST is in units of degrees Celsius. The relationships between SST and the effective upwelling and downwelling atmospheric physical temperature specified in Eq. (4) are based on a similar relationship developed by Wentz (1983).

The total brightness temperature observed from orbit is given by (Ulaby et al. 1981)

$$T_B = T_{B,\text{UP}} + [(T_c e^{-\tau} + T_{B,\text{DOWN}})(1 - \varepsilon_p) + \varepsilon_p \text{SST}]e^{-\tau}, \quad (5)$$

where SST is the sea surface temperature in units of kelvins and T_C, the cold space background brightness temperature, is approximately 6 K at L band and is varied parametrically in the study described below.

3. Simulation database

The potential performance of quasi-stationary statistical calibration methods is evaluated by simulating the global distribution of measurements that would be made by an orbiting L-band radiometer. Global distributions of SST and SSS are provided by the National Oceanic and Atmospheric Administration's (NOAA) National Oceanographic Data Center's *World Ocean Atlas 1998* (*WOA98*; Conkright et al. 1998). *WOA98* contains (among many other data products) objectively analyzed global fields of SST and SSS on a 1° × 1° grid by season during 1998. The seasons are divided as winter (January–March), spring (April–June), summer (July–September), and fall (October–December) based on the Northern Hemisphere. Also included are estimates of the standard deviations of SST and SSS during each season and for each 1° × 1° grid point. The method for objectively analyzing measured data products to produce these gridded fields is described in Levitus et al. (1994a–c).

Some of the features of the *WOA98* average SST and SSS fields are seen in Fig. 3, which plots the fields versus latitude during fall 1998. Coldest SST values (approximately −2°C) appear in both the northern and southern polar regions of Fig. 3a. Highest SSS values within the polar regions (which should combine to yield the lowest T_B values) occur in the Southern Hemisphere in Fig. 3b. Finally, Fig. 3c plots SST versus SSS for the fall 1998 global fields. The cluster of points in the lower-right-hand corner of the scatter diagram (combining low SST with high SSS) should produce the lowest values of T_B. The *WOA98* fields for the standard deviation of SST and SSS have global mean values of 1.03°C and 0.25 psu, respectively, when grid points without values are ignored. The SST and SSS standard deviations are assumed to equal these average values at grid points without values.

The global distribution of integrated water vapor is also generally dependent on latitude. A simple model for the mean value of this distribution is used of the form

→

FIG. 3. SST (a) latitude, (b) SSS vs latitude, and (c) SSS versus SST from *WOA98* objectively analyzed ocean fields on 1° × 1° grid for fall 1998.

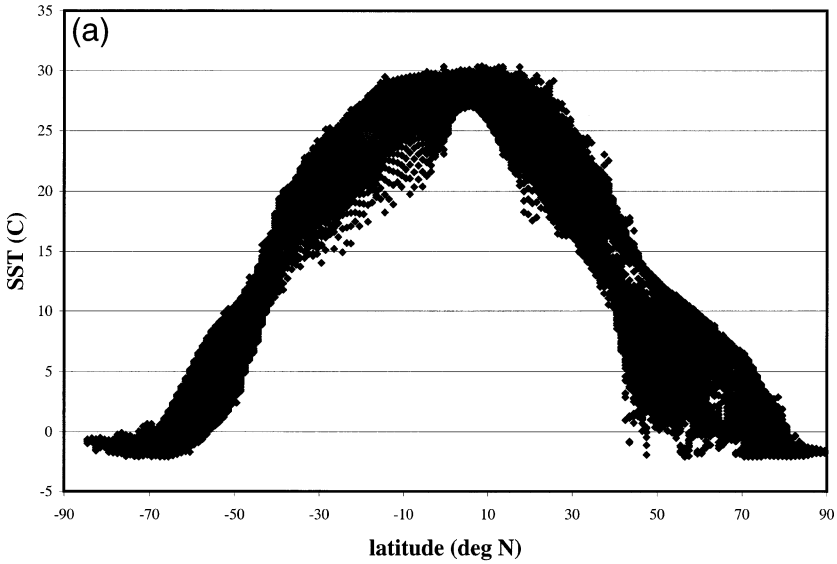
(a)
SST (C)
35
30
25
20
15
10
5
0
-5
-90 -70 -50 -30 -10 10 30 50 70 90
latitude (deg N)

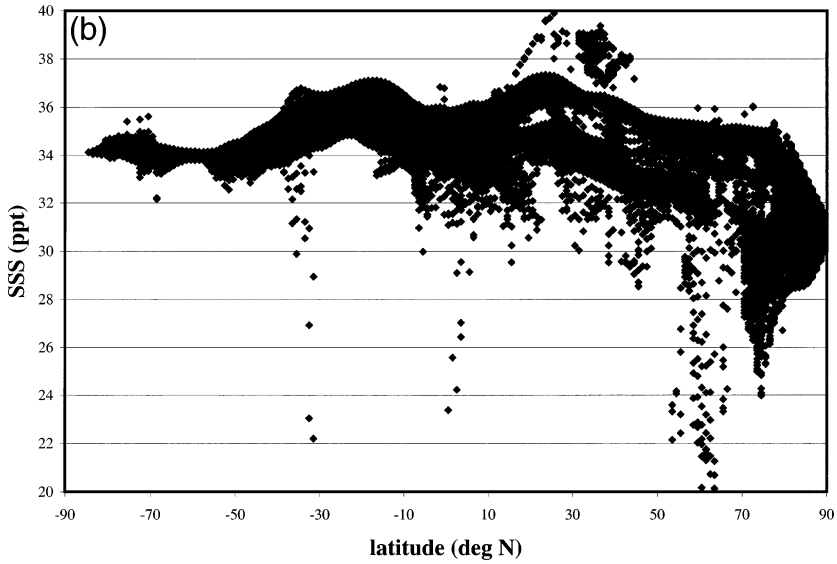
(b)
SSS (ppt)
40
38
36
34
32
30
28
26
24
22
20
-90 -70 -50 -30 -10 10 30 50 70 90
latitude (deg N)

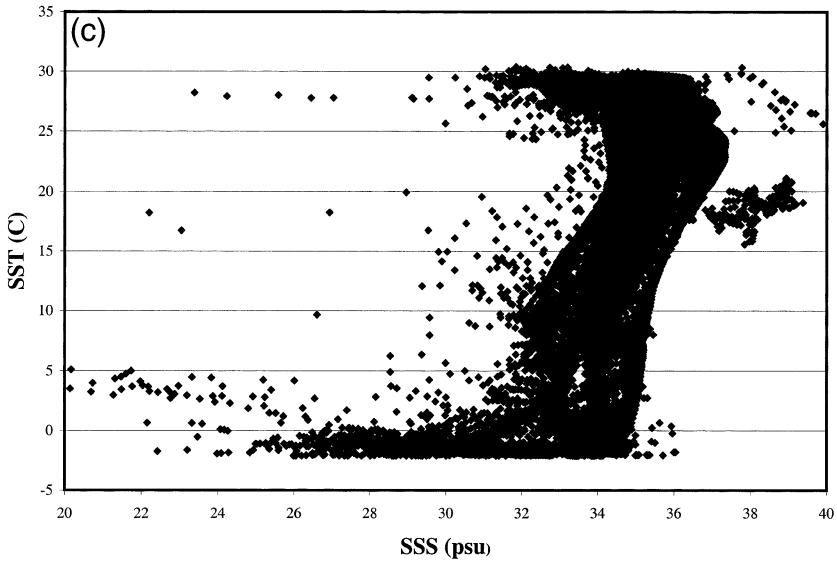
(c)
SST (C)
35
30
25
20
15
10
5
0
-5
20 22 24 26 28 30 32 34 36 38 40
SSS (psu)

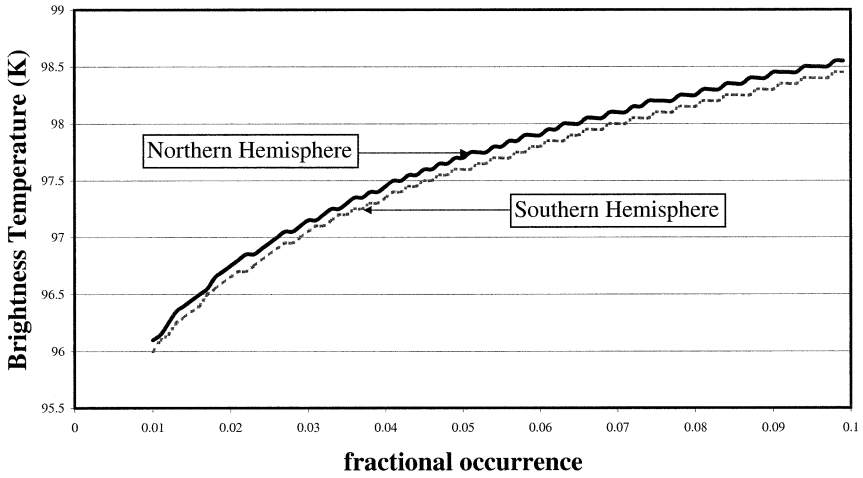

FIG. 4. ICDFs of T_B for L band at 0° incidence angle during fall 1998 for the Northern and Southern Hemispheres.

$$V = 1.0 + 3.0 \cos(\theta_{\mathrm{LAT}}) \quad (6)$$

where V is in units of centimeters and θ_{LAT} is the latitude. Equation (6) represents the mean value of V. During simulation runs (described in detail below), the value of V is allowed to vary randomly with each realization by assuming a Gaussian distribution with standard deviation equal to one-half the mean value. The allowed values for V are truncated at $V = 0$.

4. T_B simulations and sensitivity studies

Numerous simulations were run to assess the statistical calibration methods. Each realization of the simulation consists of the generation of a global distribution of T_B measurements that a low-earth-orbiting L-band radiometer might be expected to observe under specified conditions. Simulations were performed independently at off-nadir incidence angles of 0°, 20°, and 40° and for cases of vertical, horizontal, and first Stokes linear polarizations.

The conditions were varied in numerous ways to assess their impact on the stability of the statistics. Potential calibration statistics considered include the minimum, average, maximum, and vicarious cold T_B. A description of the algorithms used to estimate each statistic is given in appendix A. The nominal conditions for the simulations are summarized in appendix B. In all sensitivity studies except the second one described below (section 4b), only the fall 1998 *WOA98* database is used.

a. Assessment of confidence limits of the simulation

The confidence with which estimates of the various statistics (minimum, average, maximum, and vicarious cold T_B) can be made is first assessed by examining repeated trials of the simulation. Ten trials were run of the nominal simulation at 0°, 20°, and 40° incidence angles and with a vertical, horizontal, and 45° slant linear (first Stokes) polarization. For each trial, the T_B statistics were evaluated, after which their standard deviations over the 10 trials were computed. The average T_B is most repeatable, with standard deviations significantly below 0.01 K. The vicarious cold T_B is repeatable at the ~0.02 K level for all angles of incidence. The minimum and maximum T_B values are significantly less repeatable, with standard deviations as large as 2 K. This is to be expected, given the large number of coupled random perturbations to T_B that are being applied. Note also that the estimates of the vicarious cold and average T_B standard deviations agreed closely between polarizations at 0° incidence (at which angle there is no polarization sense and the results should, therefore, be identical). This indicates that the confidence limits themselves have been accurately estimated (i.e., the error bars on the error bars are small).

b. Sensitivity to season

The effect of season on stability was assessed by independently performing the simulations at each of the four *WOA98* seasonal databases. The results indicate that both the vicarious cold and average T_Bs are insensitive to seasonal changes in global climatology at the level of a few hundredths of kelvins. It is for this reason that all of the other simulations presented here are, without significant loss of generality, performed for the fall season only.

c. Sensitivity to latitude band

The dependence of the T_B statistics on geographical region was assessed by performing the simulations over 1) the Southern Hemisphere only, 2) the midlatitudes (45°S–45°N) only, 3) the Northern Hemisphere only, and 4) all latitudes together. The results for average T_B

TABLE 1a. The T_B statistics at 0° incidence, for fall 1998, at all latitudes, with variable sea surface wind speed.

	Nominal wind speed (m s^{-1})	50% greater wind speed (m s^{-1})
Vicarious cold T_{Bh}	95.41	95.74
Min T_{Bh}	88.58	88.68
Avg T_{Bh}	101.63	102.60
Max T_{Bh}	121.69	123.25
Vicarious cold T_{Bv}	95.41	95.74
Min T_{Bv}	90.78	91.40
Avg T_{Bv}	101.64	102.61
MaxT_{Bv}	120.35	121.64
Vicarious cold T_{B1}	95.41	95.74
Min T_{B1}	88.14	88.19
Avg T_{B1}	101.63	102.60
Max T_{B1}	122.35	123.25

TABLE 1b. The T_B statistics at 20° incidence, for fall 1998, at all latitudes, with variable sea surface wind speed.

	Nominal wind speed (m s^{-1})	50% greater wind speed (m s^{-1})
Vicarious cold T_{Bh}	91.55	91.90
Min T_{Bh}	86.72	86.85
Avg T_{Bh}	98.26	99.64
Max T_{Bh}	118.04	120.06
Vicarious cold T_{Bv}	100.55	100.90
Min T_{Bv}	95.11	95.30
Avg T_{Bv}	106.44	107.40
MaxT_{Bv}	126.94	128.30
Vicarious cold T_{B1}	96.55	96.90
Min T_{B1}	89.35	89.60
Avg T_{B1}	102.35	103.52
Max T_{B1}	123.34	125.06

indicate a statistically significant lowering of average T_B levels in the Southern Hemisphere. The difference in average T_B between the Northern and Southern Hemisphere results ranges between ~0.2 and 0.3 K versus incidence angle and polarization. This is consistent with the results presented in sections 1 and 3 above. The cold, high-salinity southern polar regions tend to produce lower T_Bs than their northern polar counterparts. The vicarious cold T_B is less sensitive to this characteristic difference between hemispheres. Differences between the Northern and Southern Hemisphere results are at most 0.1 K and are generally considerably lower. This relative insensitivity results because the 0% extrapolation procedure effectively adjusts to variations in the statistical T_B distribution between hemispheres. These results are illustrated in Fig. 4, which shows the two ICDFs that are produced in the Northern and Southern Hemispheres for the case of a 0° angle of incidence. Note in the figure that the Northern Hemisphere produces warmer T_Bs at all probabilities of occurrence but that the difference between hemispheres decreases as the probability drops. It is this tendency that allows the vicarious cold T_B method to adjust to changes in histograms and provide a more stationery statistic. In this case, the vicarious cold T_Bs are 95.46 and 95.41 K in the Northern and Southern Hemispheres whereas the average T_Bs, which do not compensate for the changes, are 101.73 and 101.55 K, respectively.

d. Sensitivity to range of SST

A second, surrogate, test of sensitivity to geographic region was performed by comparing the results using all SST values to those using only SSTs below +10°C. This effectively combines both northern and southern high-latitude bands. The intent is to assess the effects of including the larger variations in joint statistics of SST and SSS present in the north. At the lower angles of incidence, average T_B values shift down by ~0.2 K between all SST and cold SST cases. At 40° incidence, the T_{Bv} and T_{B1} averages decrease by 0.4–0.5 K. In general, V-pol T_Bs at higher angles of incidence tend to become increasing sensitive to the physical temperature of the surface (as emissivity increases), and so the greater sensitivity of the average T_B to this SST screening is to be expected. A similarly large shift in average T_B was seen in the isolated midlatitude results of section 4c, above. The vicarious cold T_Bs are less sensitive to the SST screen. Shifts in vicarious T_B are all in the neighborhood of or less than 0.1 K.

e. Sensitivity to atmosphere water vapor burden

Sensitivity to the level of atmospheric water vapor was assessed by doubling the mean water vapor burden assumed in the simulation, or

$$V = 2.0 + 6.0 \cos(\theta_{\mathrm{LAT}}), \tag{7}$$

where V is in units of centimeters and θ_{LAT} is the latitude. The standard deviation of V (equal to one-half the mean in the nominal simulation) was correspondingly doubled as well. The results suggest that water vapor burden has

TABLE 1c. The T_B statistics at 40° incidence, for fall 1998, at all latitudes, with variable sea surface wind speed.

	Nominal wind speed (m s^{-1})	50% greater wind speed (m s^{-1})
Vicarious cold T_{Bh}	79.36	79.73
Min T_{Bh}	73.02	73.07
Avg T_{Bh}	86.64	88.41
Max T_{Bh}	102.84	105.91
Vicarious cold T_{Bv}	116.36	116.73
Min T_{Bv}	111.24	111.27
Avg T_{Bv}	123.42	124.38
MaxT_{Bv}	144.73	146.38
Vicarious cold T_{B1}	97.36	97.73
Min T_{B1}	88.17	88.21
Avg T_{B1}	105.02	106.39
Max T_{B1}	125.30	127.65

TABLE 2a. The T_B statistics at 0° incidence, for fall 1998, at all latitudes, with variable variability in background cold space brightness.

	Nominal T_C variability (0.6-K rms)	Double T_C variability (1.2-K rms)
Vicarious cold T_{Bh}	95.41	95.17
Min T_{Bh}	88.58	89.38
Avg T_{Bh}	101.63	101.63
Max T_{Bh}	121.69	122.15
Vicarious cold T_{Bv}	95.41	95.17
Min T_{Bv}	90.78	90.52
Avg T_{Bv}	101.64	101.64
MaxT_{Bv}	120.35	120.62
Vicarious cold T_{B1}	95.41	95.17
Min T_{B1}	88.14	87.46
Avg T_{B1}	101.63	101.64
Max T_{B1}	122.35	122.55

TABLE 2b. The T_B statistics at 20° incidence, for fall 1998, at all latitudes, with variable variability in background cold space brightness.

	Nominal T_C variability (0.6-K rms)	Double T_C variability (1.2-K rms)
Vicarious cold T_{Bh}	91.55	91.30
Min T_{Bh}	86.72	86.27
Avg T_{Bh}	98.26	98.26
Max T_{Bh}	118.04	117.99
Vicarious cold T_{Bv}	100.55	100.30
Min T_{Bv}	95.11	94.62
Avg T_{Bv}	106.44	106.44
MaxT_{Bv}	126.94	126.99
Vicarious cold T_{B1}	96.55	96.30
Min T_{B1}	89.35	88.69
Avg T_{B1}	102.35	102.35
Max T_{B1}	123.34	123.29

only a very small impact on the stability of either the vicarious cold or average T_B values. Changes in either are well below 0.1 K in all cases.

f. Sensitivity to ocean surface winds

The nominal variation in near-surface wind speed is assumed to be uniformly distributed between 0 and 20 m s^{-1}. (This is a fairly conservative model because it introduces considerably more variation into the T_B ensemble than would a more realistic Rayleigh distributed model.) The dependence of the vicarious cold T_B on the wind conditions is assessed by considering a case where wind is uniformly distributed between 0 and 30 m s^{-1}. This would, for example, address the validity of this calibration approach during a period of time with anomalously stormy weather on a global scale. The results are summarized for each of the three incidence angles of 0°, 20°, and 40° as Tables 1a–c, respectively. Within each table, results are listed separately for the three polarizations (vertical, horizontal, and 45° slant linear) and for each statistical measure of stability (vicarious cold, minimum, average, maximum T_B). The results show a clear and statistically significant effect on both vicarious cold and average T_B levels. Vicarious cold T_B levels are increased by 0.3–0.4 K due to the higher wind conditions. Average T_B levels are increased by 1.0–1.8 K. Two points concerning these results are noteworthy. First, significant storm activity, particularly in the higher-latitude regions that contribute most to the ICDF at low probabilities of occurrence, can alter the vicarious cold T_B by a magnitude likely unacceptable to a climatological salinity mission. Second, the globally averaged T_B is much more significantly affected by anomalously high wind conditions. This greater sensitivity should, however, be qualified by noting that a global-scale increase in winds would be required to have such a large effect on the globally averaged T_B whereas a more regional increase in winds near the low SST/high SSS locations would be sufficient to impact the vicarious cold T_B.

g. Sensitivity to variability of cold space brightness

The nominal model for variations in the cold space brightness temperature downwelling onto the top of the atmosphere, T_C, is a zero mean additive Gaussian random variable with a standard deviation of 0.6 K. The mean value of T_C is assumed to be 6.0 K. The dependence of the T_B statistics on T_C is assessed by considering a case where the standard deviation is increased to 1.2 K. The results in Table 2 show a strong effect on the vicarious cold T_B but not on the average T_B. Vicarious cold T_B is lowered by ~0.2–0.3 K with the increased variability in T_C. Average T_B, on the other hand, is hardly affected at all, with changes of a few hundredths of kelvins at most. The effect on the vicarious cold T_B follows from its emphasis on the coldest T_Bs present in the database. The contribution by T_C to T_B at all levels of brightness is essentially an additive bias.

TABLE 2c. The T_B statistics at 40° incidence, for fall 1998, at all latitudes, with variable variability in background cold space brightness.

	Nominal T_C variability (0.6-K rms)	Double T_C variability (1.2-K rms)
Vicarious cold T_{Bh}	79.36	79.09
Min T_{Bh}	73.02	72.22
Avg T_{Bh}	86.64	86.64
Max T_{Bh}	102.84	103.14
Vicarious cold T_{Bv}	116.36	116.09
Min T_{Bv}	111.24	110.57
Avg T_{Bv}	123.42	123.42
MaxT_{Bv}	144.73	144.97
Vicarious cold T_{B1}	97.36	97.09
Min T_{B1}	88.17	87.44
Avg T_{B1}	105.02	105.03
Max T_{B1}	125.30	125.56

Thus, decrease in T_C will tend to lower the T_Bs and, hence, also lower the vicarious cold T_B derived from them. Increases in T_C, on the other hand, will produce higher T_Bs, which are shifted away from the coldest T_Bs and therefore have less of an effect on the vicarious cold T_B. Thus, even though the variations imposed on T_C are distributed evenly between increases and decreases, the effect of the decreases on the vicarious T_B is much greater than that of the increases. The average T_B, on the other hand, weights variations in T_C in an unbiased way and is largely unaffected by greater variability in T_C.

The sensitivity to T_C has important ramifications, for the successful use of the vicarious cold T_B as a stable calibration reference and for the success of spaceborne ocean salinity missions in general. For this reason, a sky map of T_C, including variations about the big bang background continuum due, for example, to the galactic plane and neutral hydrogen line emission will be incorporated into the future Soil Moisture and Ocean Salinity Mission (SMOS) and Aquarius satellite data processing (Kerr 1998; Koblinsky 2002). Such a map may also be needed to compensate for the effects of T_C variations on the vicarious cold T_B since the locations at which the coldest T_B samples are measured can vary with the ocean surface wind speed and salinity and with the atmospheric opacity fields.

h. Sensitivity to variability of SSS and SST

The standard deviations of the average SST and SSS fields used in the nominal simulations are provided as a *WOA98* data product. Average standard deviations over the full global field are 1.03°C and 0.25 psu. The dependence of the vicarious cold reference on the level of SST and SSS variability is tested by considering a case with twice the *WOA98* variability. The results indicate that, while the minimum T_Bs have been very significantly lowered and the maximum T_Bs moderately increased, the effect on both vicarious cold and average T_Bs is not significant.

5. Effects of sample size—Data record length requirements

The simulation results presented in section 4 all assume that 10 independent measurements were made at each 1° × 1° grid in latitude and longitude over the globe. This would, for example, be roughly consistent with data accumulated over a time sufficient to image the entire earth by a sensor having three independent cross-track samples of 30-km resolution each at a single incidence angle. The dependence of the stability of the average and vicarious cold T_B on sensor type and record length is addressed by considering two specific sensor designs. The SMOS sensor is a spaceborne radiometer currently in phase B fabrication by the European Space Agency. It will have roughly 40 km cross-track by 20 km along-track spatial resolution, a swath width of 560 km, and a per-sample ΔT of 2.0 K (Kerr 1997). This results in 14 independent cross-track samples every 20 km of along-track motion, which produces approximately 70 independent samples for every 1° change in latitude due to orbital motion. Aquarius is a planned spaceborne sensor that includes an L-band radiometer that is under development by the National Aeronautics and Space Administration (NASA) Goddard Space Flight Center and the Jet Propulsion Laboratory (Koblinsky 2002). It makes a single independent measurement every 28 km of along-track motion with a ΔT of 0.06 K. This results in approximately three independent samples per 1° change in latitude. Thus, the SMOS sensor has ~23 times more samples but each of its sample is ~33 times noisier. The relative merits of these two characteristics are evaluated here.

The effect of record length on the stability of the T_B statistics is evaluated by selecting subsets of the full 180° × 360° global grid for processing. Using the complete set of grid points corresponds to the case of full earth coverage. In a single day for typical low-earth orbits, roughly 14 complete orbit revolutions will be made. In terms of the global grid of SST and SSS data, this corresponds to sampling the grid over all latitudes but in increments of approximately 13° in longitude. This results in a subset of the global grid with 12° gaps in longitude and 0° gaps in latitude. Similarly, a 2-day record length could be represented by a subset with 6° gaps in longitude, etc. (The exact correspondence between record length and longitude gap size depends more precisely on orbit inclination and altitude, but this approximation is sufficient for illustrative purposes.) Numerical simulations were performed in which a subset of the global grid was used. The subset is specified by the gap size in longitude. For a given gap size, a complete set of T_Bs was simulated according to either the SMOS or Aquarius design parameters. The average and vicarious cold T_Bs were then computed. This was repeated 100 times (each time randomly selecting the lowest longitude in the subset to be between 1° and the gap size). The standard deviation of the 100 average and vicarious cold T_Bs represents the stability of that statistic. The results are summarized in Figs. 5 and 6.

Figure 5a shows the stability of the SMOS first Stokes brightness vicarious cold T_B estimate for varying record lengths. The results for this and all of the following stability tests were similar at horizontal and vertical linear polarization. Using a 1-day record length (corresponding to 12° gaps in longitude coverage), the vicarious cold T_B has a ~0.1 K standard deviation. The stability improves to ~0.05 K using a 2-day record (6° gaps) and continues to drop with lengthening time record, reaching 0.01–0.02 K with full earth coverage. This behavior can be interpreted in terms of its impact on potential operational use of the cold reference by considering the variability due to record length as one component of a comprehensive accuracy budget that accounts for all sources of variability. For example, if

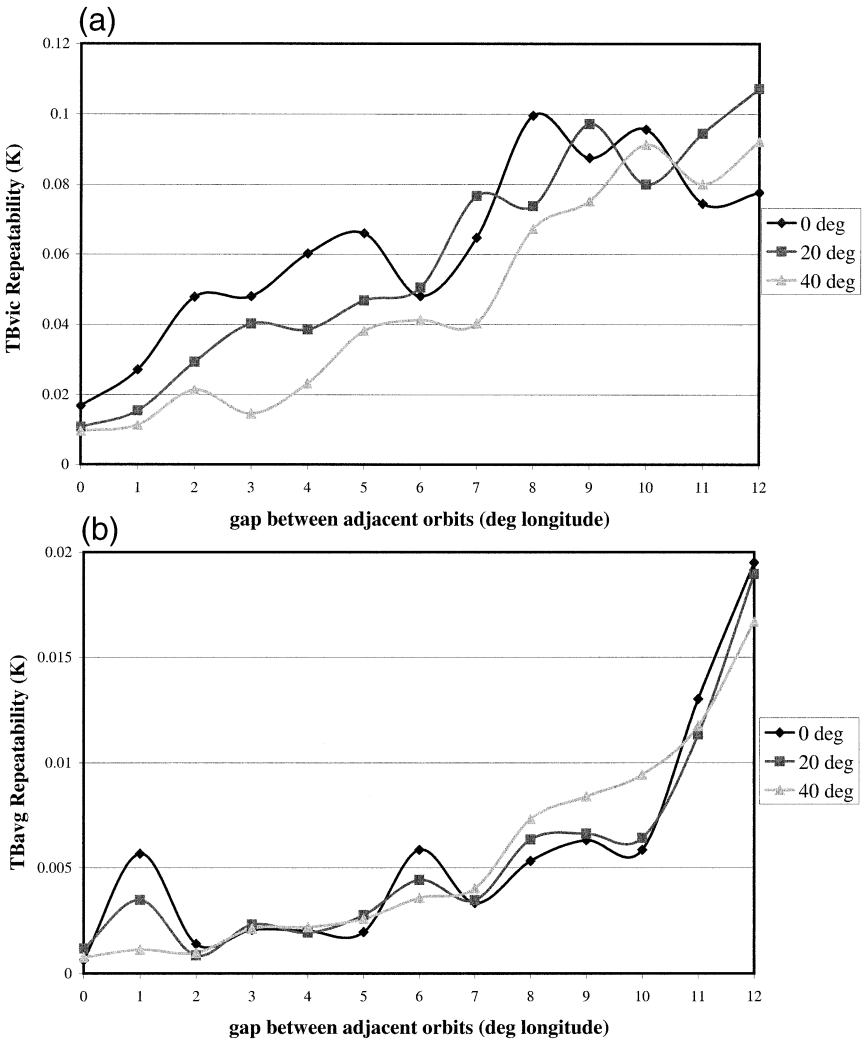

FIG. 5. Stability of the (a) vicarious cold T_B and (b) average T_B for first Stokes pol applied to the SMOS sensor parameters vs earth coverage (or, equivalently, vs database record length).

the most stable calibration reference possible is desired, then full earth coverage should be included in the dataset. In this case, the 0.01–0.02-K stability predicted in Fig. 5a would likely only be a small component of the total accuracy budget. Variations due to high wind speeds or changes in T_C may well dominate the error budget in this case. If, on the other hand, daily estimates of the cold reference are needed, then the overall accuracy budget could be significantly impacted by the 0.1-K stability predicted in Fig. 5a. Such a degraded accuracy budget might be justified if, for example, the onboard sensor calibration standards tended to drift on timescales of 1 day to a greater extent than the overall accuracy of the cold reference. The cold reference could, then, be used to calibrate the onboard standards on a daily schedule and the onboard standards would be used to calibrate the raw T_B measurements on shorter timescales.

Figure 5b shows the stability of the SMOS average T_B for varying record lengths. This statistic is extremely stable even with short (daily or subdaily) record lengths. It is likely that a comprehensive accuracy budget for the average T_B would be dominated by other sources of variation with 1 day or even shorter records. The other sources of variation should, then, be given paramount consideration when deciding what record length to use. For example, while record lengths of less than 1 day may have more than an adequate sample size to guarantee repeatability of the average statistic, they are also more likely to include anomalous weather conditions that can bias the average statistic since anomalies tend to have short timescales.

Figure 6 shows stability results using the Aquarius sensor parameters. The results are qualitatively similar to those for SMOS but differ markedly in magnitude. The Aquarius vicarious cold T_B standard deviation is roughly 3 times that of SMOS. The Aquarius average T_B is roughly twice as variable versus record length.

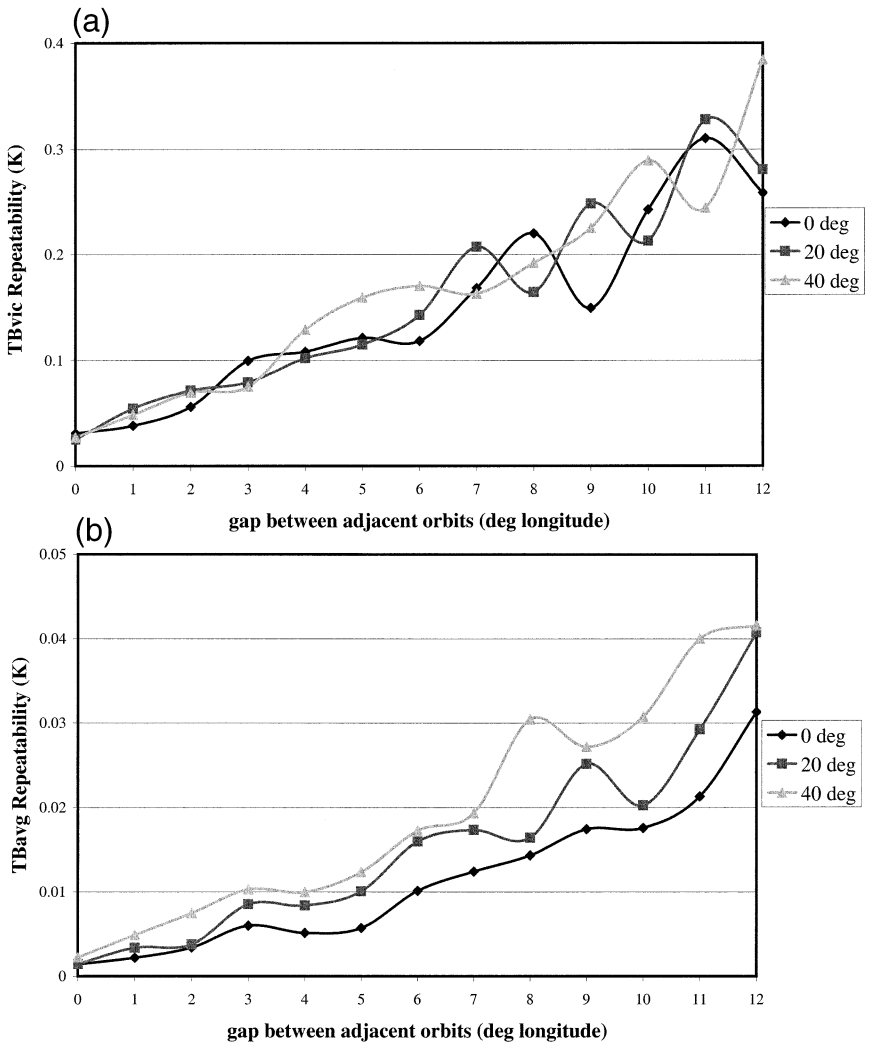

FIG. 6. Stability of the (a) vicarious cold T_B and (b) average T_B for first Stokes pol applied to the Aquarius sensor parameters vs earth coverage (or, equivalently, vs database record length).

Recall that SMOS had 33 times the noise and only 23 times the number of samples. If the stability of these statistics was driven simply by the noise in each sample, then SMOS would be more variable by roughly $33/23^{1/2} \approx 7$. In fact, it is 2 to 3 times less variable. These results suggest that, in both the vicarious cold and average T_B cases, a large number of independent realizations of the geophysical state is much more beneficial than is a very low noise floor on each individual realization. These results should, however, be qualified by noting that one key assumption about the environmental parameters that were varied in the simulation was that they had independent realizations for each sample in the ensemble of T_B measurements. There will likely be some correlation between variations in water vapor burden, wind speed, SST, and SSS at sample separations of 1° latitude or less. The result would be a decrease in the effective number of independent samples accumulated per unit time and a corresponding decrease in the stability of the statistics under investigation. This would be especially relevant in the case of SMOS, which will have roughly a 23 times higher spatial sampling density than Aquarius.

6. Conclusions and discussion

A simulator has been developed to assess the sensitivity of the vicarious cold and average T_B statistics to variations in numerous environmental factors that alter the statistical distribution of T_Bs that would be measured by an earth-viewing L-band radiometer. It is found that the average T_B is relatively insensitive (effected at or below the ~0.1 K level) to changes in season, water vapor burden, cold space brightness, and SSS and SST variability. The vicarious cold T_B is similarly insensitive to season, water vapor burden, and SSS and SST variability, as well as to the selective filtering of data by

Northern versus Southern Hemisphere and by cold versus all SST values.

The average T_B shifts by 0.2–0.3 K (depending on incidence angle and polarization) when averaged individually over the Northern versus the Southern Hemisphere. Selectively filtering out only the coldest SST values (below +10.0°C) has a negligible effect on the average T_B except at vertical and the first Stokes polarizations with higher (e.g., 40°) angles of incidence. In those cases, the average T_B increases by ~0.4 K. Increasing the distribution of near-surface wind speeds has a dramatic effect on the globally averaged T_B. A 50% increase in the globally distributed wind speed produces a 1.0–1.8-K increase in the average.

The vicarious cold T_B is also affected by increases in the wind speed distribution, although to a lesser extent. A 50% increase in wind speed results in a 0.3-K increase in the vicarious cold T_B. It should be noted that the vicarious cold T_B can be affected even if the increase in wind speed is confined to isolated regions of the earth (e.g., those with the lowest SST and highest SSS values that produce the coldest surface T_B measurements). Such a regional increase in wind speeds is probably more likely to occur than is the global increase that would be needed to produce the 1.0–1.8-K increase in globally averaged T_B. The vicarious cold T_B is much more affected by variations in the background cold space brightness, T_C, than is the average. A decrease in the vicarious cold T_B by 0.3 K results from an increase in rms variability of T_C from 0.6 to 1.2 K about an assumed mean value of 6.0 K. This sensitivity suggests that a correction to the vicarious cold T_B may be needed in practice if the distribution of the background T_C values that are present during the coldest T_B observations changes appreciably.

The fact that the average and vicarious cold T_B statistics tend to vary for different reasons—high winds and varying T_C, respectively—suggests that using both statistics as calibration references should be mutually beneficial. Potential drifts in onboard sensor calibration constants would ideally be identified by consistent comparisons against both statistics. If the two statistics indicated different sensor drifts, then the characteristics of the T_B ensemble from which the statistics were derived could be examined in greater detail. In the case of the average T_B, the globally averaged wind speed over the period of the data record could be estimated from numerical weather fields and compared to its typical value. The average wind speed over restricted regions with low SST and high SSS could also be used to assess its impact on the vicarious cold T_B. The low SST–high SSS regions could also be examined with regard to the average and standard deviation of T_C values observed by the sensor in a specular direction. Significant variations of these T_C statistics would indicate potential variations in the cold reference statistic.

The size of the data ensemble that is required to estimate reliable statistics was also examined. The average T_B is found to require a considerably smaller data sample than does the vicarious cold T_B. Daily accumulations of data are more than sufficient to eliminate sample size as a source of variation in the average, whereas vicarious cold T_Bs that are derived daily will include a component of variability due to sample size that is roughly comparable to other sources of variation in the statistic due to natural geophysical variability. The dependence on sample size has been examined for the simplifying case of uncorrelated samples; in practice, environmental parameters affecting the samples will be partially correlated and larger sample sizes will be required to provide equivalent levels of stationarity in the statistics.

In practice, the use of these T_B statistics to track and correct for instabilities in a radiometer will depend heavily on details of the sensor design and the approach used by its calibration algorithm. The experience with TMR is described in Ruf (2002). A small, long-term drift in the isolation of a critical calibration switch at 18 GHz was corrected using the vicarious cold T_B as an absolute reference. In the case of upcoming L-band spaceborne missions, both SMOS and Aquarius rely on the stability of internal noise diodes as calibration standards. Small, long-term drifts either in their noise output or in the interconnections that couple their noise power into the radiometer could presumably be tracked and corrected using the T_B statistics described here. In addition, other (unforeseen) problems with radiometer stability would hopefully also produce significant, detectable effects on the statistics.

Acknowledgments. The results presented here grew out of work begun while on a visiting appointment in the Department of Electromagnetic Systems at the Danish Technical University (DTU). The author is grateful to DTU and to his host, Professor Niels Skou, for providing the resources and the inspiration to begin this study. Many useful comments and suggestions were also offered by the anonymous reviewers and have been incorporated. The author also gratefully acknowledges use of the SST and SSS distributions provided by the NOAA/National Oceanographic Data Center *World Ocean Atlas for 1998.*

APPENDIX A

Procedural Steps for Deriving Relevant Statistics from the T_B Ensemble

Each run of the simulator produces an ensemble of realizations of T_B measurements that incorporates variations in environmental parameters (water vapor burden, ocean surface wind speed, and background cold space brightness) superimposed over a global distribution of values for SST and SSS and including additive zero mean measurement noise. Details of the forward model used to generate the T_Bs are given in section 2 above. From this ensemble, a set of statistics is derived.

a. Standard T_B statistics

The minimum, average, and maximum values of T_B were derived from the ensemble of T_B measurements by conventional statistical analysis. The minima and maxima are the coldest and hottest T_B in the ensemble. The average is the arithmetic mean.

b. Vicarious cold T_B statistic

Given an ensemble of T_B measurements, the vicarious cold T_B is derived by extrapolating the ICDF corresponding to that ensemble back to the highest T_B with 0% occurrence. The extrapolation is performed by curve fitting a third-order polynomial in x to ICDF(x) and then evaluating the polynomial at $x = 0$. Specifically, as follows:

1) Order the T_Bs from lowest to highest. Find the T_B below which 1.0% of all realizations lie—call it ICDF(1.0); find the T_B below which 1.1% of all realizations lie—call it ICDF(1.1); continue up to ICDF(10.0). (Using this method of construction, the ICDF is guaranteed to be monotonic.)
2) Arrange the ICDFs into vector form as $\mathbf{y}$, where y_1 = ICDF(1.0), y_2 = ICDF(1.1), . . . , y_{91} = ICDF(10.0).
3) Define a third-order polynomial regression matrix, $\mathbf{P}$, by

$$P_{ij} = (0.9 + 0.1i)^j, \tag{A1}$$

where $i = 1, 1, \ldots, 91$ and $j = 0, 1, 2, 3$.
4) The assumption of a third-order polynomial relationship between x and ICDF(x) is equivalent to assuming the model $\mathbf{y} = \mathbf{Pc}$, where $\mathbf{c}$ is a four-element vector of regression coefficients. The coefficients are found by minimizing the squared error between $\mathbf{y}$ and $\mathbf{Pc}$, or

$$\mathbf{c} = (\mathbf{P}^T\mathbf{P})^{-1}\mathbf{P}^T\mathbf{y}. \tag{A2}$$

5) Evaluation of the polynomial approximation to ICDF at $x = 0\%$ is equivalent to selecting the zeroth regression coefficient. In other words, the vicarious cold T_B equals c_0.

APPENDIX B

Nominal State of Radiometer Hardware and Environmental Parameters for Simulation of T_B Ensemble

1) The T_B measurements are free of biases due to calibration errors.
2) The T_B measurements are corrupted by zero mean additive Gaussian noise with a standard deviation (ΔT) of 2.0 K.
3) The background cold space brightness temperature downwelling onto the top of the atmosphere, T_C, is assumed to be Gaussian distributed with a mean value of 6.0 and a standard deviation of 0.6 K. Individual realizations that fall below 2.7 K are truncated there. Each individual calculation of the T_B measured by the radiometer includes an independent realization of T_C.
4) Near-surface wind speed, u (as it affects the ocean emissivity), is assumed to be uniformly distributed between 0 and 20 m s^{-1}. Each individual calculation of the T_B measured by the radiometer includes an independent realization of u.
5) Integrated water vapor burden, V, in the atmosphere is assumed to be Gaussian distributed with a mean value given by Eq. (6) and a standard deviation equal to one-half the mean. The allowed values for V are truncated at $V = 0$. Each individual calculation of the T_B measured by the radiometer includes an independent realization of V.
6) Global distributions of SST and SSS follow the *WOA98* fields. Both variables are assumed to be Gaussian distributed with mean values and standard deviations specified by the corresponding *WOA98* databases. Each individual calculation of the T_B measured by the radiometer includes an independent realization of SST and SSS. At each latitude–longitude point on the $1° \times 1°$ grid, 10 independent realizations of T_B are generated.

REFERENCES

Blume, H. J. C., A. W. Love, M. J. Van Melle, and W. W. Ho, 1977: Radiometric observations of sea temperature at 2.65 GHz over the Chesapeake Bay. *IEEE Trans. Antennas Propag.*, **25,** 121–128.

Conkright, M., S. Levitus, T. O'Brien, T. Boyer, J. Antonov, and C. Stephens, 1998: *World Ocean Atlas 1998* CD-ROM data set documentation. NODC Tech. Rep. 15, Silver Spring, MD, 16 pp.

Ellison, W., A. Balana, G. Delbos, K. Lamkaouchi, L. Eymard, C. Guillou, and C. Prigent, 1998: New permittivity measurements of seawater. *Radio Sci.*, **33,** 639–648.

Kerr, Y., 1998: SMOS-MIRAS on RAMSES: Radiometry applied to soil moisture and salinity measurements (full proposal). A.O. Earth Explorer Opportunity Missions, European Space Agency, 97 pp.

Klein, L. A., and C. T. Swift, 1977: An improved model for the dielectric constant of sea water at microwave frequencies. *IEEE Trans. Antennas Propag.*, **25,** 104–111.

Koblinsky, C. J., 2002: Aquarius ocean salinity mission. NASA Earth System Science Pathfinder Missions Proposal, 26 pp.

Lagerloef, G., C. Swift, and D. LeVine, 1995: Sea surface salinity: The next remote sensing challenge. *Oceanography*, **8,** 44–50.

Le Vine, D. M., M. Kao, R. W. Garvine, and T. Sanders, 1998: Remote sensing of ocean salinity: Results from the Delaware Coastal Current experiment. *J. Atmos. Oceanic Technol.*, **15,** 1478–1484.

Levitus, S., and T. P. Boyer, 1994: *Temperature*. Vol. 4, *World Ocean Atlas 1994*, NOAA Atlas NESDIS 4, 117 pp.

——, R. Burgett, and T. P. Boyer, 1994a: *Salinity*. Vol. 3, *World Ocean Atlas 1994*, NOAA Atlas NESDIS 3, 99 pp.

——, R. Gelfeld, T. P. Boyer, and D. Johnson, 1994b: Results of the NODC and IOC Oceanographic Data Archaeology and Rescue Project. World Ocean Atlas 1994 Rep. 1, 64 pp.

Ruf, C. S., 2000: Detection of calibration drifts in spaceborne microwave radiometers using a vicarious cold reference. *IEEE Trans. Geosci. Remote Sens.*, **38,** 44–52.

——, 2002: Characterization and correction of a drift in calibration of the TOPEX microwave radiometer. *IEEE Trans. Geosci. Remote Sens.,* **40,** 509–511.

Stogryn, A., 1997: Equations for the permittivity of sea water. Naval Research Laboratory Tech. Rep. Code 7113, PO-570122, 11 pp.

Swift, C. T., and R. E. McIntosh, 1983: Considerations for microwave remote sensing of ocean-surface salinity. *IEEE Trans. Geosci. Remote Sens.,* **21,** 480–491.

Ulaby, F. T., R. K. Moore, and A. K. Fung, 1981: Radiometry. *Microwave Remote Sensing, Active and Passive.* Vol. 1, Addison-Wesley, 456 pp.

Wentz, F. J., 1983: A model function for ocean microwave brightness temperatures. *J. Geophys. Res.,* **88** (C3), 1892–1908.

Yueh, S. H., R. West, W. J. Wilson, F. K. Li, E. G. Njoku, and Y. Rahmat-Samii, 2001: Error sources and feasibility for microwave remote sensing of ocean surface salinity. *IEEE Trans. Geosci. Remote Sens.,* **39,** 1049–1060.